Bull. Mater. Sci., Vol. 27, No. 4, August 2004, pp. 333–336. © Indian Academy of Sciences.

Bridgman growth and defects of Nd^{3+} : $Sr_3Ga_2Ge_4O_{14}$ laser crystals

JIAXUAN DING, ANHUA WU and JIAYUE XU*

Shanghai Institute of Ceramics, Chinese Academy of Sciences, Shanghai 200050, PR China

MS received 23 April 2004

Abstract. **Nd^{3+} : $Sr_3Ga_2Ge_4O_{14}$ crystals have been grown by the modified Bridgman method. The growth defects, such as striations, scattering particles and dislocations were investigated. Some featherlike striations were observed in as-grown crystals. EPMA analysis suggested that these inclusions were caused by the segregation of Nd_2O_3 from the melt. Chemical etching results showed that the dislocation density was in the range of $10^3 \sim 10^5/cm^2$.**

Keywords. **Nd^{3+} : SGG crystal; Bridgman method; EPMA; inclusion; dislocation.**

1. Introduction

Ca-gallogermanate ($Ca_3Ga_2Ge_4O_{14}$) type laser crystals have attracted much attention due to their disordered structure. $Sr_3Ga_2Ge_4O_{14}$ (SGG) is one of Ca-gallogermanate type crystals with a = 8·270(3) Å, c = 5·040(1) Å, $a = b = 90°$, g = 120 (Kaminsky *et al* 1984), and has a transmittance of more than 80% in the range 350–2500 nm. It was found that the dopant, Nd^{3+} ions, experienced a disordered crystal field, resulting in macroscopic inhomogeneous line broadening of the absorption and luminescence spectra due to the statistically distributed Ga^{3+} and Ge^{4+} cations in the crystallographic site in SGG crystals (Kaminsky *et al* 1984). The broadened absorption bands improved the pumping efficiencies, while the increased luminescence linewidths enabled large wavelength tuning ranges and the possibility to obtain very short laser pulses, similar to those with laser Nd^{3+} : glasses. On the other hand, the disordered crystals exhibited almost the same thermal conductivity as the Nd^{3+} : $Y_3Al_5O_{12}$ garnet. This made the laser operation with higher repletion rate possible (Eichler *et al* 1994). Therefore, Nd^{3+} ions doped Ca-gallogermanate ($Ca_3Ga_2Ge_4O_{14}$) type crystals may possess both the advantages of laser Nd^{3+} : glasses and laser crystal Nd^{3+} : $Y_3Al_5O_{12}$ garnet.

So far, all of pure SGG and Nd^{3+} : SGG crystals had been grown by Czochralski method. Due to the volatilization of GeO_2 component, the crystals grown by Czochralski method were small and the crystal quality was not so good. Recently, pure SGG crystals up to Φ28 × 60 mm had been grown successfully by the modified vertical Bridgman method for piezoelectric applications (Zhou *et al* 2004). In this paper, Nd^{3+} : SGG single crystals were grown by the modified Bridgman method and the growth defects were investigated by EPMA and chemical etching.

2. Crystal growth

Polycrystalline SGG raw materials were synthesized by solid-phase reaction. High purity $SrCO_3$ (99·99%), Ga_2O_3 (99·999%) and GeO_2 (99·999%) were weighed at the molar ratio of $SrCO_3 : Ga_2O_3 : GeO_2 = 3 : 1 : 4$ and mixed thoroughly in an agate mortar. The mixture was sintered in a muffle furnace at 1100°C for 16 h. Figure 1 shows powder X-ray diffraction pattern of the sintered mixture that was identical to that of SGG crystal in JCPDS card. The dopant Nd_2O_3 of different concentrations was mixed thoroughly with the SGG powder. Then, they were charged into a Pt crucible with a <001>-oriented SGG seed at the bottom. The crucible was sealed and moved to a refractory tube filled with Al_2O_3 powder. A pair of Pt–Pt/Rh thermocouples was installed in the tube to measure the temperature of the melt near the top of the seed. The Bridgman growth was carried out in a homemade Bridgman furnace. A DWT-702 fine temperature controller with precision of ± 0·5°C was used to control the furnace temperature. The furnace temperature was set to 1450°C, which was 50°C higher than the melting point of SGG. Using <001>-oriented SGG seeds, SGG crystals doped with 1·5, 3, 8, 12 at% Nd^{3+} were grown. In order to get high doping concentration of Nd^{3+} : SGG crystal, we initially grew 12 at% Nd^{3+} : SGG. However, the growth ceased when about 1/3 melt became transparent crystal. The crystal doped with 1·5 at% Nd^{3+} was easily grown and inclusion-free 8 at% Nd^{3+} : SGG crystal up to Φ25 × 40 mm was obtained. Figure 2 shows as-grown SGG crystal doped with 8 at% Nd^{3+}. The crystal was covered with a layer of pale pink impurities. The impurity covers were

*Author for correspondence

observed in all Nd^{3+} : SGG crystals of different Nd^{3+} concentrations.

3. Defect characterizations

3.1 *Striations*

As mentioned above, as-grown Nd^{3+} : SGG crystals were covered with a layer of pale pink impurities. In order to test growth defects, the crystals were polished. Featherlike striations were easily observed by naked eyes. Figure 3 shows the typical featherlike striations, which extended from the shouldering part to the tail of the crystal. The space between striations is about 1 mm. The crystal including the striations was cut and polished for analysis. A Shimadzu-8705QH2 electron probe microanalyser (EPMA) with a link INCA Energy (Oxford Instruments, UK) energy spectrum analyser was used to give the secondary electron (SE) image and back scattering electron (BSE) image and determine the elemental composition of the inclusions. Figure 4 shows the morphology of the striation by EPMA. The compositions in areas A and B are listed in table 1. Area A represents the transparent crystal and its compositions are very close to theoretical values. However, the compositions of area B show a Nd_2O_3-rich striation. A textured structure was observed in the striation region, as shown in figure 4. It suggested that Nd_2O_3-rich solution crystallized when it was frozen in the crystal.

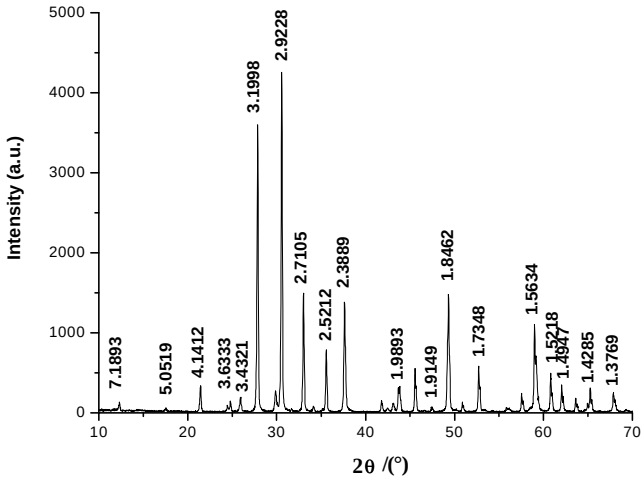

Figure 1. Powder X-ray diffraction pattern of SGG polycrystalline obtained by solid-state reaction.

Figure 2. As-grown SGG crystals doped with 8 at% Nd^{3+} ions covered with impurities.

3.2 *Scattering particles*

The inclusions, including striations and scattering particles, were usually found at the tail part of as-grown crystals. The striations were easily observed while the scattering particles were tested by means of He–Ne laser beam. The crystal was cut into a plate of 1 mm thickness where scattering particles were found. The polished samples were observed by metallurgical microscope. The scattering particles displayed different shapes. The cloud-like inclusions were made up of fine fibres of 1μm in diameter and the whole size was about 20 × 20 μm. The sizes of belt-like and tube-like inclusions were about 8 μm in diameter and 300 ~ 500 μm in length.

The distribution coefficient of Nd^{3+} in SGG crystal was measured as 0·57 in our previous work (Ding *et al* 2004).

Table 1. Chemical composition result of Nd^{3+}: SGG crystal with EPMA study.

	Ga_2O_3	GeO_2	SrO	Nd_2O_3
Melt	20·15	44·98	33·42	1·45
A	18·18	45·81	34·85	1·16
B	3·55	33·73	26·70	36·03

Figure 3. Featherlike striations in as-grown Nd^{3+} : SGG crystal.

This meant that more Nd_2O_3 segregated in the melt during the later stage of the growth. The Nd_2O_3-rich inclusion formed when the temperature in solid–liquid interface fluctuated. In order to obtain high quality Nd^{3+} : SGG crystals, precise control of the furnace temperature and slow growth rate were adopted.

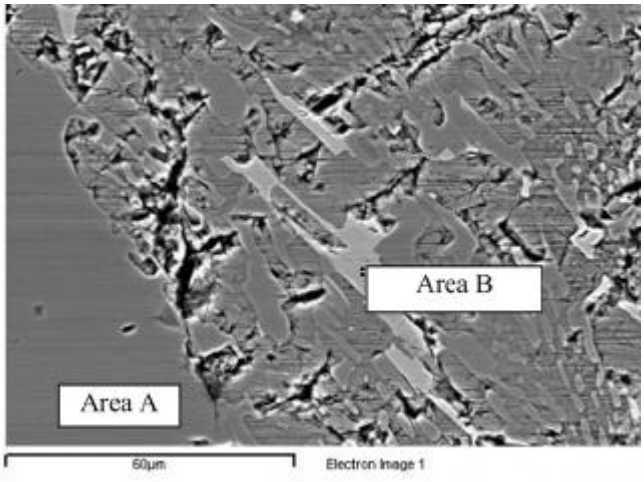

Figure 4. Morphology of the inclusions in Nd^{3+} : SGG crystal.

3.3 *Dislocations*

Because of lack of literature on chemical etching of SGG crystal, several acids were attempted. An etchant with the volume ratio of $H_3PO_4 : H_2O = 2 : 1$ was adopted. The samples of transparent Nd^{3+} : SGG crystals were oriented as <001>, <201> and <111> and polished for chemical etching. The samples were immersed in the etchant at 80–100°C for 10–15 min. The etched samples with these low-index planes were observed under the metallurgical microscope. Generally, the symmetry of an etch pit was in accordance with the symmetry of the crystal face, and the shapes of etch pits on different faces were different for the same crystal (Sang 1987). Figure 5 shows the etch pits of (001), (201) and (111) planes. The etch pits of the dislocations on (001) and (201) planes were triangular, but

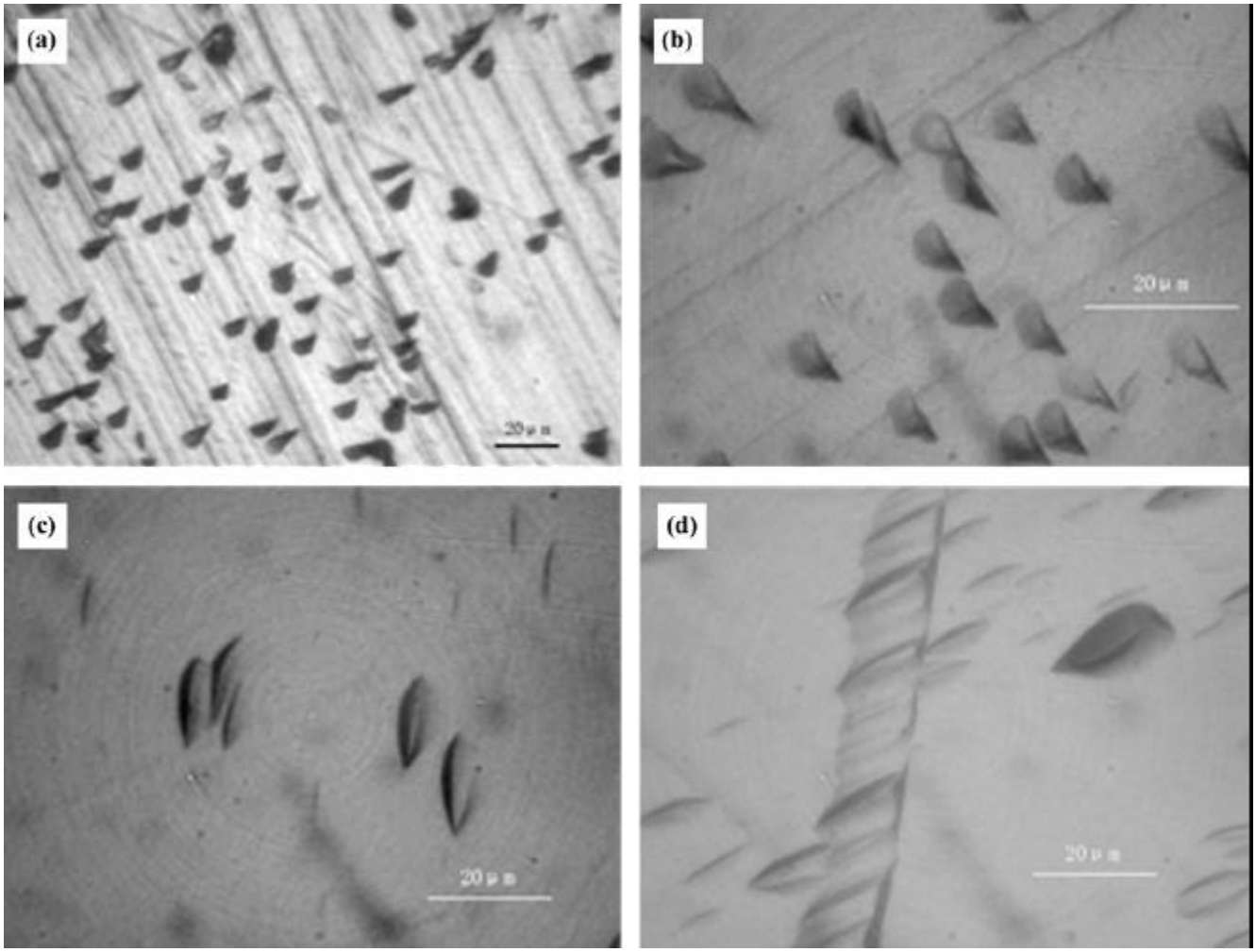

Figure 5. The etch pits of Nd^{3+} : SGG crystal. The etch pits distribution on **(a)** (001) plane, **(b)** (201) plane, **(c)** (111) plane and **(d)** (111) plane of Nd^{3+} : SGG crystals.

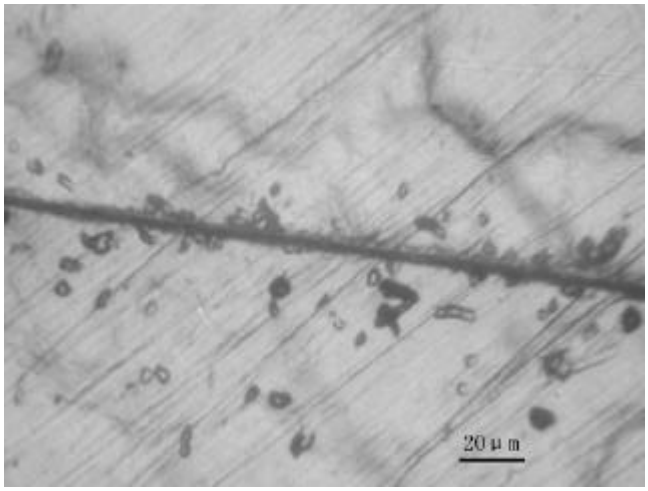

Figure 6. The distribution of etch pits near the micro-crack.

those on the (111) plane were spindle-like. These etch patterns were related to the trigonal crystal system of Nd^{3+} : SGG crystal. Figure 5(d) shows some dislocation lines in (111) plane. No dislocation lines were observed in (001) and (201) planes. The etch pit density of the transparent Nd^{3+} : SGG crystal was calculated to be $10^3 \sim 10^5/cm^2$.

The growth dislocations in crystal might originate from the following sources: (i) dislocations already existed in the seed; (ii) dislocations produced by nucleation at the seed-crystal interface, where some defects such as mechanical damage of the seed surface, aggregation of impurity particles and inclusions, and thermal stress do exist; (iii) dislocations emerging from the impurity particles and inclusions trapped within the crystal during crystal growth and (iv) dislocations caused by macro defects. Figure 6 shows etch pits near the crack in (201) plane. A large number of dislocations assemble near the crack.

4. Conclusions

$Sr_3Ga_2Ge_4O_{14}$ crystals doped with 1·5, 3, 8, 12 at% Nd^{3+} were grown by the vertical Bridgman method. The growth defects such as striations, scattering particles and dislocations were investigated. Featherlike striations and scattering particles with different shapes were observed in as-grown crystals. EPMA analysis suggested that these inclusions are caused by the segregation of Nd_2O_3 from the melt. Chemical etching results show that the dislocation density is in the range of $10^3 \sim 10^5/cm^2$.

References

Ding Jiaxuan, Wu Anhua, Zhou Juan, Xu Jiayue and Fan Shiji 2004 *J. Synth. Cryst.* **33** 346

Eichler H J, Ashkenasi D, Jian H and Kaminsky A A 1994 *Phys. Status Solidi* **(a)146** 833

Kaminsky A A, Belokoneva E L, Mill B V, Pisarevskii Y V, Sarkisov S E, Silvestrova I M, Butashin A V and Khodzhabagyan G G 1984 *Phys. Status Solidi* **(a)86** 345

Sang S 1987 *Etching of crystal theory, experiment and application* (Amsterdam: North-Holland) p. 303

Zhou J, Xu J Y, Wu A H and Fan S J 2004 *Mater. Sci. & Eng.* **B106** 213